Distortion Compensation of Reconstructed Hologram Image in Digital Holographic Display Based on Viewing Window

Minsik Park, Hyun-Eui Kim, Hyon-Gon Choo, Jinwoong Kim, and Cheong Hee Park

A holographic display based on a viewing window enables the converging of a reconstruction wave into a viewing window by means of an optical system. Accordingly, a user can observe a reconstructed hologram image, even with a small diffraction angle. It is very difficult to manufacture an optical system with no aberrations; thus, it is inevitable that a certain amount of wave aberrations will exist. A viewing-window-based holographic display, therefore, always includes distortions in an image reconstructed from a hologram pattern. Compensating the distortions of a reconstructed image is a very important technical issue because it can dramatically improve the performance when reconstructing a digital three-dimensional content image from a hologram pattern. We therefore propose a method for suppressing image distortion by measuring and compensating the wave aberration calculated from a Zernike polynomial, which can represent arbitrary wave aberrations. Through our experimental configuration using only numerical calculations, our proposed method decreased the reconstructed image distortion by more than 28%.

Keywords: Holographic display, Wave aberration, Zernike polynomial.

Manuscript received Apr. 20, 2016; revised Apr. 11, 2017; accepted May 8, 2017.

Minsik Park (pms@etri.re.kr), Hyun-Eui Kim (turnn@etri.re.kr), Hyon-Gon Choo (hyongonchoo@etri.re.kr), and Jinwoong Kim (jwkim@etri.re.kr) are with the 5G Giga Communication Research Laboratory, ETRI, Daejeon, Rep. of Korea.

Cheong Hee Park (corresponding author, cheonghee@cnu.ac.kr) is with the Department of Computer Science and Engineering, Chungnam National University, Daejeon, Rep. of Korea.

I. Introduction

A holographic digital display provides users with a realistic three-dimensional (3D) image or video by manipulating the hologram pattern, which represents the wave field of a 3D object. A spatial light modulator (SLM), a core device of a holographic digital display, loads a hologram pattern to reconstruct a 3D object in a free space. An SLM such as a liquid crystal display (LCD), digital micro-mirror device (DMD), or liquid crystal on silicon (LCoS) can be implemented as a display panel. Existing commercial panels do not satisfy SLM performance with a wide-viewing zone angle to observe a reconstructed image from the hologram displayed on the SLM with the naked eye. This is because the current state of technology does not enable the manufacturing of a display panel with a sub-micro-pixel pitch. Several alternative approaches exist to address the limited viewing zone angle of an existing SLM using scanning multiplexing [1], [2], tiling multiplexing [3]–[5], and a viewing window [6], [7].

Among these methods, a holographic display based on a viewing window allows even an LCD with a large pixel pitch to realize a sufficiently wide viewing angle. Such a display, however, has a disadvantage in that a reconstructed hologram is geometrically distorted by wave aberrations that are introduced by the converging optical system for generating a viewing window [7]. The converging optical system in a viewing-window holographic display cannot avoid wave aberrations according to Siedel aberrations if it is designed and implemented using only spherical surfaces [8].

Studies have been conducted on exploiting a complex wave field phase [9]–[12] and applying an affine

geometrical transformation to a hologram [13]–[17] to correct a distorted image numerically reconstructed from a hologram in the field of digital holography. We chose an approach to change the phase information from a hologram to compensate optical system wave aberrations in the viewing-window holographic display. The renowned approach to changing a phase is to use both a wavefront sensor (or an optical interferometer) that can quantitatively measure wave aberrations and a deformable mirror that controls a physical surface in a random form [18], [19].

The wave aberrations can be mathematically represented using Zernike polynomials [20], [21], that is, a set of orthonormal functions. Zernike polynomials can be obtained through a wave aberration measurement, such as a Shack-Hartmann sensor [22] and interferometry [23]. A Shack-Hartmann sensor consists of a two-dimensional (2D) lenslet array and a charge-coupled device (CCD) sensor. Interferometry includes a reference optical system to generate a reference wave for interfering with an object wave propagated from a test optical system. A viewing-window holographic display is generally composed of a converging optical system with a large aperture to illuminate a large-sized SLM. The effective area of a Shack–Hartmann sensor is too small for measuring such a large aperture. Moreover, interferometry incurs a significant expense and effort for preparing a large-sized reference optical system. The measured wave aberrations of an optical system are compensated by a wave aberration compensator, such as a deformable mirror [24], [25] that can change its physical surface with an arbitrary shape. A wave aberration compensator also has a problem in handling a large aperture because its effective aperture is small, similar to a wave aberration measurement.

A method is therefore required for easily measuring and compensating wave aberrations with no limitation on the aperture size of a converging optical system in a viewing-window holographic display. Ray tracing is very useful in measuring wave aberrations of an optical system with a large aperture because it can numerically calculate the Zernike coefficient from a given design specification of an optical system, even if a wave aberration measurement is not established. The obtained wave aberrations can be transformed into a compensation phase field, which is applied to a viewing-window holographic display [6], [7].

In this paper, we propose a method for decreasing the distortion of a reconstructed image from a hologram pattern in a viewing-window holographic display using only numerical calculations for measuring and compensating aberrations introduced from the converging optical system. To this end, a numerical diffraction model of a viewing-window holographic display is derived and the Zernike coefficients are obtained from the wave aberrations of the converging optical system through ray tracing.

The remainder of this paper is organized as follows. Section II describes an approach of representing a wave aberration using Zernike polynomials, and Section III deduces a diffraction model for a numerical hologram reconstruction and generation in a viewing-window holographic display. In Section IV, the experimental results illustrating the distortion suppression of the reconstructed images achieved through the proposed method are provided.

II. Wave Aberration Representation

A normalized Zernike polynomial $Z_n^m(\rho,\theta)$ composed of a normalization term N_n^m a radial term $R_n^{|m|}(\rho)$ and a sinusoidal term $\phi(\theta)$ is defined in (1) [10]. Here, ρ and θ indicate the radius and azimuthal angle, respectively, in polar coordinates, where θ is measured in a counterclockwise direction from the $+x$ axis. The subscript n and superscript m of Z indicate the order and frequency of a Zernike polynomial, respectively, where n is greater than or equal to zero, and the absolute value of m is less than or equal to n. Moreover, n and m are either odd or even.

$$Z_n^m(\rho,\theta)=\left\{\begin{array}{c} N_n^m\times R_n^{|m|}(\rho)\times\cos(m\theta)\ \text{for}\ m\geqslant 0 \\ -N_n^m\times R_n^{|m|}(\rho)\times\sin(m\theta)\ \text{for}\ m<0 \end{array}\right\}. \tag{1}$$

The sinusoidal term in (1) is selected with a cosine function if the frequency m is greater than or equal to zero, and with a sine function for all other cases.

The radial term $R_n^{|m|}(\rho)$ is calculated according to (2), and is dependent on m, n, and ρ.

$$R_n^{|m|}(\rho)=\sum_{s=0}^{\frac{n-|m|}{2}}\frac{(-1)^s(n-s)!}{s!\left[\frac{(n+|m|)}{2}-s\right]!\left[\frac{n-|m|}{2}-s\right]!}\rho^{n-2s}. \tag{2}$$

A Zernike polynomial consisting of both a radial term and a sinusoidal term is an orthogonal, not an orthonormal, function. It requires the additional term in (3) for normalization.

$$N_n^m = \sqrt{\frac{2(n+1)}{(1+\delta_{m,0})}}\ (\delta_{m,0} = 1 \text{ if } m = 0, \delta_{m,0} = 0 \text{ if } m \neq 0). \tag{3}$$

The wave aberration function used to sum Zernike polynomial $Z_n^m(\rho,\theta)$ multiplied by coefficient W_n^m can represent any arbitrary wave aberration.

$$W(\rho,\theta) = \sum_{n=0}^{\infty}\sum_{m=-n}^{n} W_n^m Z_n^m(\rho,\theta). \tag{4}$$

In (5), Zernike polynomial coefficient W_n^m is obtained from an integral equation of the wave aberration function $W(\rho, \theta)$ multiplied by Zernike polynomial $Z_n^m(\rho,\theta)$.

$$W_n^m = \frac{1}{\pi}\int_0^1 \int_0^{2\pi} W(\rho,\theta)\cdot Z_n^m(\rho,\theta) d\theta\rho d\rho. \tag{5}$$

The wave aberration field $P(\rho, \theta)$ is represented using the wave aberration function $W(\rho, \theta)$ in (6).

$$P(\rho,\theta) = e^{-j\frac{2\pi}{\lambda}W(\rho,\theta)}$$

or

$$P(x,y) = e^{-j\frac{2\pi}{\lambda}W(x,y)}. \tag{6}$$

The polar coordinate (ρ, θ) can be converted into the Cartesian coordinate (x, y) by replacing (ρ, θ) with $(\sqrt{x^2+y^2}, \tan^{-1}(y/x))$.

III. Diffraction Model in Viewing-Window Holographic Display with Wave Aberration

1. Diffraction Model without Converging Optical System

It is useful to simulate the observation condition of a human eye using a diffraction model in a viewing-window holographic display. This is because it can numerically simulate the same reconstruction image as a user, or a camera that can obtain from a wave field propagated from an SLM to a user retina or camera sensor in a free space. The simple observation model of a human eye is composed of a pupil, an eye lens, and a retina, as shown in Fig. 1. The pupil acts as a viewing-window of a wave field on a pupil plane, the eye lens as a convex lens with a variable focal length according to the distance of an object plane, and the retina serves as an image plane. A camera

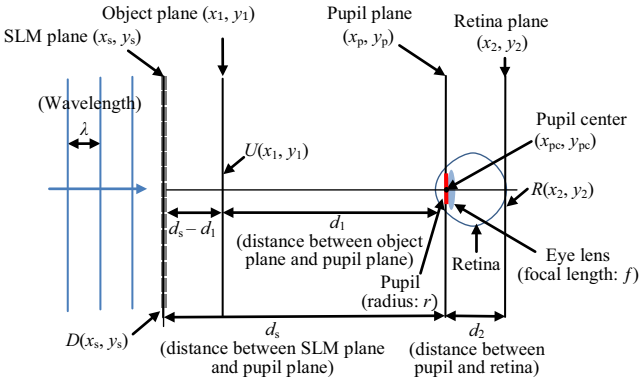

Fig. 1. Diffraction model based on the observation model of a human eye or camera.

aperture corresponds to a pupil, a camera lens correlates to an eye lens, and a camera sensor is analogous to a retina when a camera captures a hologram image reconstructed in a free space.

Figure 1 shows a diffraction model, which includes an observation model of a human eye without converging optics on an SLM plane when using a collimated plane wave as an illumination.

A wave field $D(x_s, y_s)$ on an SLM plane (x_s, y_s) as an input hologram propagates into a wave field $R(x_2, y_2)$ on a retina plane (x_2, y_2) through a wave field $U(x_1, y_1)$ on an object plane (x_1, y_1) Here, $D(x_s, y_s)$ is a hologram pattern, a wave field inputted in the SLM plane of a holographic display; λ is defined as the wavelength of an illumination; d_1 is the distance between an object plane (x_1, y_1) and a pupil plane (x_p, y_p); d_2 is the distance between a pupil plane (x_p, y_p) and a retina plane (x_2, y_2); d_s is the distance between an SLM plane (x_s, y_s) and a retina plane (x_2, y_2); and f is the focal length of an eye lens.

The focal length f of an eye lens or a camera is calculated by (7), which is derived from the formula of the lens-maker if a user or camera focuses on an object plane (x_1, y_1) placed between the SLM plane (x_s, y_s) and retina plane (x_2, y_2).

$$\frac{1}{d_1} + \frac{1}{d_2} = \frac{1}{f}, \quad f = \frac{d_1 d_2}{d_1 + d_2}. \tag{7}$$

Here, $R(x_2, y_2)$ on the retina plane (x_2, y_2) is propagated from $D(x_s, y_s)$ on the SLM plane (x_s, y_s) according to the diffraction model defined in Fig. 1. Equation (8), which shows the diffraction relationship between $R(x_2, y_2)$and $D(x_s, y_s)$, is derived from the optical geometry with a positive lens placed between the source plane and the target plane, as described in [26].

https://doi.org/10.4218/etrij.17.0116.0049

$$
\begin{aligned}
R(x_2,y_2)=&\exp\left\{j\frac{2\pi(x_2^2+y_2^2)}{\lambda\quad 2d_2}\right\}\\
&\times\int_{-\infty}^{\infty}\int PL(x_{pc},y_{pc},r)\\
&\qquad\exp\left\{j\frac{2\pi}{\lambda}\left(\frac{1}{d_s}+\frac{1}{d_2}-\frac{1}{f}\right)\left(\frac{x_p^2+y_p^2}{2}\right)\right\}\\
&\times\left[\int_{-\infty}^{\infty}\int D(x_s,y_s)\exp\left\{j\frac{2\pi(x_s^2+y_s^2)}{\lambda\quad 2d_s}\right\}\right.\\
&\qquad\left.\exp\left\{-j2\pi\left(\frac{x_p}{\lambda d_s}x_s+\frac{y_p}{\lambda d_s}y_s\right)\right\}dx_sdy_s\right]\\
&\times\exp\left\{-j2\pi\left(\frac{x_2}{\lambda d_2}x_p+\frac{y_2}{\lambda d_2}y_p\right)\right\}dx_pdy_p.
\end{aligned}
\tag{8}
$$

A pupil aperture function $PL(x_{pc}, y_{pc}, r)$ is defined with a *circ* function of (9), where (x_{pc}, y_{pc}) and r are the center coordinate and radius of the eye lens in the pupil plane, respectively. Here, $PL(x_{pc}, y_{pc}, r)$ is used to describe a situation in which an eye is shifted in the pupil plane.

$$
\begin{aligned}
PL(x_{pc},y_{pc},r)&=\mathrm{circ}\left\{\frac{(x_p-x_{pc})^2+(y_p-y_{pc})^2}{r^2}\right\}\\
&=\begin{cases}1 & \dfrac{(x_p-x_{pc})^2+(y_p-y_{pc})^2}{r^2}<1\\[2ex] \dfrac{1}{2} & \dfrac{(x_p-x_{pc})^2+(y_p-y_{pc})^2}{r^2}=1\\[2ex] 0 & \dfrac{(x_p-x_{pc})^2+(y_p-y_{pc})^2}{r^2}>1.\end{cases}
\end{aligned}
\tag{9}
$$

Figure 1 does not consider a converging optic, which is composed of a convex lens and a point light source. A converging optic is used to implement a viewing-window digital holographic display that enables a user to observe the image reconstructed from a hologram with the naked eye despite a very narrow diffraction angle.

Figure 2 shows a diffraction model in a complete optical system of a viewing-window digital holographic display. The position of the viewing window on the pupil plane is moved according to the position of the point light source.

2. Diffraction Model with Converging Optical System

The spherical wave field emitted from a point source functions as the reconstructed beam and illuminates the SLM plane through the converging optical system, which acts as a convex lens. The SLM modulates the spherical wave field according to a hologram pattern in order to reconstruct a 3D object in a free space. There are two kinds of modulated wave fields departing from the SLM plane. The first is a non-diffracted wave field in an on-axis hologram to be focused on one point on the pupil plane, which is located at a distance d_s away from the SLM plane. The other is a diffracted wave field of a zero order that is used to form a viewing window. A user can observe the reconstructed 3D object by placing an eye over the viewing window.

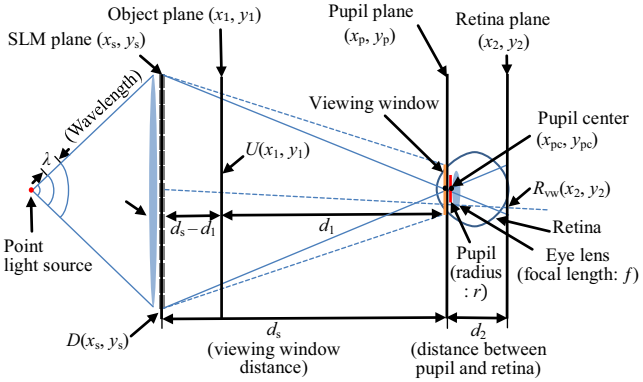

Fig. 2. Diffraction model based on a viewing window.

The converging optical system generates the converging spherical wave field $S(x_s, y_s)$ with focal length d_s, as defined in (10).

$$
S(x_s,y_s)=\exp\left\{-j\frac{2\pi}{\lambda}\frac{(x_s^2+y_s^2)}{2d_s}\right\}. \tag{10}
$$

The wave field $R_{vw}(x_2, y_2)$ is obtained by multiplying $D(x_s, y_s)$ by $S(x_s, y_s)$ in (8). The term $S(x_s, y_s)\exp\left\{j\frac{2\pi}{\lambda}\frac{(x_s^2+y_s^2)}{2d_s}\right\}$ in the second integral of (11) becomes one. Equation (11) represents the diffraction relationship between a wave field $R_{vw}(x_2, y_2)$ and a hologram pattern $D(x_s, y_s)$ in a viewing-window holographic display.

For back-propagation from the wave field $R_{vw}(x_2, y_2)$ through the pupil plane, $D(x_s, y_s)$ is derived as (12).

$$
\begin{aligned}
R_{vw}(x_2,y_2)=&\exp\left\{j\frac{2\pi(x_2^2+y_2^2)}{\lambda\quad 2d_2}\right\}\\
&\times\int_{-\infty}^{\infty}\int PL(x_{pc},y_{pc},r)\\
&\qquad\exp\left\{j\frac{2\pi}{\lambda}\left(\frac{1}{d_s}+\frac{1}{d_2}-\frac{1}{f}\right)\left(\frac{x_p^2+y_p^2}{2}\right)\right\}\\
&\times\left[\int_{-\infty}^{\infty}\int D(x_s,y_s)S(x_s,y_s)\exp\left\{j\frac{2\pi(x_s^2+y_s^2)}{\lambda\quad 2d_s}\right\}\right.\\
&\left.\times\exp\left\{-j2\pi\left(\frac{x_p}{\lambda d_s}x_s+\frac{y_p}{\lambda d_s}y_s\right)\right\}dx_sdy_s\right]\\
&\times\exp\left\{-j2\pi\left(\frac{x_2}{\lambda d_2}x_p+\frac{y_2}{\lambda d_2}y_p\right)\right\}dx_pdy_p.
\end{aligned}
\tag{11}
$$

$$
\begin{aligned}
D(x_s,y_s) = S(x_s,y_s)^{-1}\exp\left\{-j\frac{2\pi}{\lambda}\frac{(x_s^2+y_s^2)}{2d_s}\right\} \\
\times\int_{-\infty}^{\infty}\int\exp\left\{-j\frac{2\pi}{\lambda}\left(\frac{1}{d_s}+\frac{1}{d_2}-\frac{1}{f}\right)\frac{(x_p^2+y_p^2)}{2}\right\} \\
\times\left[\int_{-\infty}^{\infty}\int R_{vw}(x_2,y_2)\exp\left\{-j\frac{2\pi}{\lambda}\frac{(x_2^2+y_2^2)}{2d_2}\right\}\right. \\
\left.\times\exp\left\{j2\pi\left(\frac{x_p}{\lambda d_2}x_2+\frac{y_p}{\lambda d_2}y_2\right)\right\}dx_2dy_2\right] \\
\times\exp\left\{j2\pi\left(\frac{x_s}{\lambda d_s}x_p+\frac{y_s}{\lambda d_s}y_p\right)\right\}dx_pdy_p.
\end{aligned}
\tag{12}
$$

Here, the term $S(x_s,y_s)^{-1}exp\left\{-j\frac{2\pi}{\lambda}\frac{(x_s^2+y_s^2)}{2d_s}\right\}$ of (12) is equal to one. The wave field $R_{vw}(x_2, y_2)$ can be replaced with the wave field $U(-\frac{d_1}{d_2}x_2, -\frac{d_1}{d_2}y_2)$ scaled down $U(x_1, y_1)$ by d_2/d_1 in the $x$and y axis direction according to (13), which is derived from the diffraction relationship between $R_{vw}(x_2, y_2)$ and $U(x_1, y_1)$ of (11) if equation (7) is satisfied.

$$
\begin{aligned}
&R_{vw}\left(x_2,y_2;\ f=\frac{d_1d_2}{d_1+d_2}\right) \\
&=\exp\left\{j\frac{2\pi}{\lambda}\frac{(x_2^2+y_2^2)}{2d_2}\right\}U\left(-\frac{d_1}{d_2}x_2,-\frac{d_1}{d_2}y_2\right).
\end{aligned}
\tag{13}
$$

We can obtain $R_{vw}(x_2, y_2); f$ according to (13) if an object wave field $U(x_1, y_1)$ is given and is focused by an eye or camera lens. In addition, $D(x_s, y_s)$ is furthermore generated by substituting the obtained $R_{vw}(x_2, y_2); f$ in (12), and is the hologram pattern to be loaded on the SLM plane to optically reconstruct the object wave field $U(x_1, y_1)$.

The off-axis wave field is useful for enabling a reconstructed 3D object to be easily observed because it can spatially separate the twin hologram images to be reconstructed when SLM modulates only the amplitude of a complex wave field. The off-axis wave field $D_{shift}(x_s, y_s)$ on the SLM plane can be generated according to (14) by multiplying $D(x_s, y_s)$ by a shifting phase factor $SPF(x_s,y_s) = \exp\{j\frac{2\pi}{\lambda}(\sin\theta_{x_s}x_s + \sin\theta_{y_s}y_s)\}$. The shifting phase factor $SPF(x_s, y_s)$ is equal to that introduced by a prism with deflection angle $(\theta_{x_s}, \theta_{y_s})$ calculated from $\left(\tan^{-1}\frac{x_{pc}}{d_s}, \tan^{-1}\frac{y_{pc}}{d_s}\right)$ [27].

$$
D_{shift}(x_s,y_s) = D(x_s,y_s)\times SPF(x_s,y_s). \tag{14}
$$

$SPF(x_s, y_s)$ is defined in (15) when a shifting coordinate is equal to (x_{pc}, y_{pc}), which is the center coordinate of an eye lens in the pupil plane. $\left(\sin(\tan^{-1}\frac{x_{pc}}{d_s}), \sin(\tan^{-1}\frac{y_{pc}}{d_s})\right)$ is approximately equal to $\left(\frac{x_{pc}}{d_s}, \frac{y_{pc}}{d_s}\right)$ assuming that d_s is greater than x_{pc} and y_{pc}.

$$
SPF(x_s,y_s) = \exp\left\{j\frac{2\pi}{\lambda}\left(\frac{x_{pc}}{d_s}x_s+\frac{y_{pc}}{d_s}y_s\right)\right\}. \tag{15}
$$

The converging optical system always includes some wave aberrations because it cannot be optically designed with no such aberrations. It produces a converging spherical wave field with wave aberrations for an illumination of a viewing-window holographic display. The illumination wave field $C(x_s, y_s; x_{vc}, y_{vc})$ can be mathematically expressed as a multiplication of both $S(x_s, y_s)$ and $P(x_s, y_s; x_{vc}, y_{vc})$ in (16).

$$
C(x_s,y_s;x_{vc},y_{vc}) = S(x_s,y_s)\times P(x_s,y_s;x_{vc},y_{vc}). \tag{16}
$$

Here, $P(x_s, y_s; x_{vc}, y_{vc})$ is a wave aberration field on the SLM plane (x_s, y_s), calculated according to (6), when a viewing window is centered at a coordinate (x_{vc}, y_{vc}) in the pupil plane. The wave field leaving from the SLM plane is calculated by multiplying $D_{shift}(x_s, y_s)$ by $C(x_s, y_s; x_{vc}, y_{vc})$. Thus, the retina wave field $R'_{vw}(x_2, y_2; x_{vc}, y_{vc})$ in a viewing-window holographic display with wave aberrations is derived by replacing $D(x_s, y_s)$ and $\exp\left\{j\frac{2\pi}{\lambda}\left(\frac{1}{d_s}+\frac{1}{d_2}-\frac{1}{f}\right)\left(\frac{x_p^2+y_p^2}{2}\right)\right\}$ with $D_{shift}(x_s, y_s) \times C(x_s, y_s; x_{vc}, y_{vc})$ and $\exp\left\{j\frac{2\pi}{\lambda}\left(\frac{1}{d_s}+\frac{1}{d_2}-\frac{1}{f}\right)\left(\frac{(x_p-x_{pc})^2+(y_p-y_{pc})^2}{2}\right)\right\}$ in (8).

$$
\begin{aligned}
R'_{vw}(x_2,y_2;x_{vc},y_{vc}) = &\exp\left\{j\frac{2\pi(x_2^2+y_2^2)}{\lambda\ 2d_2}\right\} \\
&\times\int_{-\infty}^{\infty}\int PL(x_{pc},y_{pc},r) \\
&\qquad\exp\left\{j\frac{2\pi}{\lambda}\left(\frac{1}{d_s}+\frac{1}{d_2}-\frac{1}{f}\right)\left(\frac{(x_p-x_{pc})^2+(y_p-y_{pc})^2}{2}\right)\right\} \\
&\times\left[\int_{-\infty}^{\infty}\int D_{shift}(x_s,y_s)P(x_s,y_s;x_{vc},y_{vc})\right. \\
&\qquad\left.\exp\left\{-j2\pi\left(\frac{x_p}{\lambda d_s}x_s+\frac{y_p}{\lambda d_s}y_s\right)\right\}dx_sdy_s\right] \\
&\times\exp\left\{-j2\pi\left(\frac{x_2}{\lambda d_2}x_p+\frac{y_2}{\lambda d_2}y_p\right)\right\}dx_pdy_p.
\end{aligned}
\tag{17}
$$

Equation (17) is used to calculate a wave field on the retina plane if a hologram pattern $D(x_s, y_s)$ on the SLM plane and a wave aberration field $P(x_s, y_s; x_{vc}, y_{vc})$ on the converging optical system is given. This means that (17) enables us to numerically reconstruct a hologram pattern on the SLM plane in a viewing-window holographic display with wave aberrations without conducting any optical experiments.

https://doi.org/10.4218/etrij.17.0116.0049

The hologram pattern $\bar{D}(x_s, y_s; x_{vc}, y_{vc})$ of the compensating wave aberrations is generated by multiplying $D(x_s, y_s)$ by the inverse of a wave aberration field in (6) to suppress a wave aberration field $P(x_s, y_s; x_{vc}, y_{vc})$ on the converging optical system when the center of the viewing window is placed at (x_{vc}, y_{vc}) in the pupil plane.

$$\begin{aligned}\bar{D}(x_s,y_s;x_{vc},y_{vc}) &= D_{shift}(x_s,y_s)\times P(x_s,y_s;x_{vc},y_{vc})^{-1}\\ &= D(x_s,y_s)\times SPF(x_s,y_s)\\ &\quad\times P(x_s,y_s;x_{vc},y_{vc})^{-1}\end{aligned} \tag{18}$$

Here, $\bar{D}(x_s, y_s; x_{vc}, y_{vc})$ is derived in (19) with regard to $U\left(-\frac{d_1}{d_2}x_2, -\frac{d_1}{d_2}y_2\right)$ by substituting $D(x_s, y_s)$ of (12) and $R_{vw}(x_2, y_2)$ of (13) in (18) if an object wave field $U(x_1, y_1)$ is given.

$$\begin{aligned}\bar{D}(x_s,y_s;x_{vc},y_{vc}) &= SPF(x_s,y_s)\times P(x_s,y_s;x_{vc},y_{vc})^{-1}\\ &\times\int_{-\infty}^{\infty}\int\exp\left\{-j\frac{2\pi}{\lambda}\left(\frac{1}{d_s}+\frac{1}{d_2}-\frac{1}{f}\right)\frac{(x_p^2+y_p^2)}{2}\right\}\\ &\times\left[\int_{-\infty}^{\infty}\int U\left(-\frac{d_1}{d_2}x_2,-\frac{d_1}{d_2}y_2\right)\right.\\ &\left.\exp\left\{j2\pi\left(\frac{x_p}{\lambda d_2}x_2+\frac{y_p}{\lambda d_2 y_2}\right)\right\}dx_2dy_2\right]\\ &\times\exp\left\{j2\pi\left(\frac{x_s}{\lambda d_s}x_p+\frac{y_s}{\lambda d_s}y_p\right)\right\}dx_pdy_p.\end{aligned} \tag{19}$$

Equations (17) and (19) can be represented through a Fourier transform to employ a fast Fourier transform (FFT).

$$\begin{aligned}&R'_{vw}(x_2,y_2;x_{vc},y_{vc})\\ &=\exp\left\{j\frac{2\pi(x_2^2+y_2^2)}{\lambda\quad 2d_2}\right\}\\ &FT_{(x_p,y_p)}\left[PL(x_{pc},y_{pc},r)\exp\left\{j\frac{2\pi}{\lambda}\left(\frac{1}{d_s}+\frac{1}{d_2}-\frac{1}{f}\right)\right.\right.\\ &\left.\left(\frac{(x_p-x_{pc})^2+(y_p-y_{pc})^2}{2}\right)\right\}\\ &\left.\times FT_{(x_s,y_s)}\{D(x_s,y_s)SPF(x_s,y_s)P(x_s,y_s;x_{vc},y_{vc})\}\right].\end{aligned} \tag{20}$$

$$\begin{aligned}&\bar{D}(x_s,y_s;x_{vc},y_{vc})\\ &=SPF(x_s,y_s)P(x_s,y_s;x_{vc},y_{vc})^{-1}\\ &\times FT^{-1}_{(x_p,y_p)}\left[\exp\left\{-j\frac{2\pi}{\lambda}\left(\frac{1}{d_s}+\frac{1}{d_2}-\frac{1}{f}\right)\frac{(x_p^2+y_p^2)}{2}\right\}\right.\\ &\left.\times FT^{-1}_{(x_2,y_2)}\left\{U\left(-\frac{d_1}{d_2}x_2,-\frac{d_1}{d_2}y_2\right)\right\}\right].\end{aligned} \tag{21}$$

Here, $\bar{D}(x_s, y_s; x_{vc}, y_{vc})$ is the hologram pattern to be generated with respect to the single depth between the SLM plane and the object plane.

The 3D object consists of sliced object planes with different depths. The compensated volume hologram pattern $\bar{\bar{D}}(x_s, y_s; x_{vc}, y_{vc})$ is obtained as the sum of the hologram patterns generated with regard to the sliced object planes, as shown in Fig. 3. The value of $\bar{\bar{D}}(x_s, y_s; x_{vc}, y_{vc})$ is calculated according to (22) if a 3D object is divided with N-sliced object planes.

$$\bar{\bar{D}}(x_s,y_s;x_{vc},y_{vc})=\sum_{i=1}^{N}\bar{D}(x_s,y_s;x_{vc},y_{vc},z_i). \tag{22}$$

IV. Experimental Results

In our previous study [7], a converging optical system for generating a viewing window was designed to minimize any wave aberrations. It is composed of two lens groups to include a doublet lens for reducing color aberrations, as shown in Fig. 4. The point light source is replaced to change the position of the viewing window on the pupil plane according to the movement of the observer's eye. The exit pupil is designed to be placed on the center plane of the second group lens, which is 2,600 mm from the pupil plane in Fig. 4.

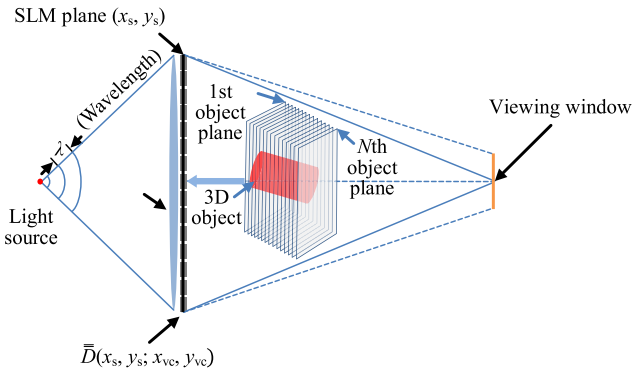

Fig. 3. Hologram pattern generation in a 3D object.

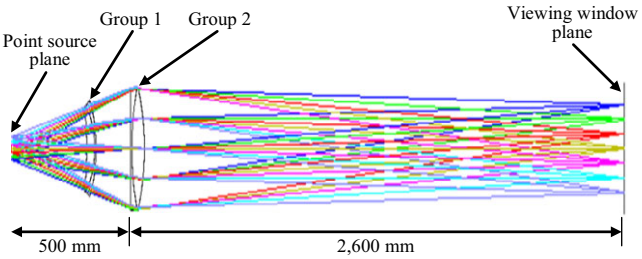

Fig. 4. Design of a converging optical system using ray tracing from a light point source into a center position of a viewing window.

Figure 5 shows the designed size of the converging optical system. The first and second class materials in group 1 are H-FK61 and N-LASF31A, respectively, and the first and second materials in group 2 are N-LASF40 and N-LAK12, respectively. The wave aberrations of a converging optical system introduce a geometric distortion in the image reconstructed from a hologram pattern displayed on the SLM.

Figure 6 illustrates our experimental configuration in which a digital single-lens reflex (DSLR) camera can capture a distorted image for optical reconstruction from a hologram pattern in a viewing-window holographic display. The configuration includes one dot chart and three rulers positioned at a distance of 0, 1,000, 1,600, and 2,200 mm, respectively, from the SLM to recognize the accommodation effect from the reconstructed image.

The SLM was implemented using a transmissive LCD panel with a resolution of 1,200 × 1,200, and a pixel pitch of 125 μm × 125 μm. The DSLR camera used was a Canon EOS 5D with a CCD sensor 35.8 mm × 35.8 mm in size and a 12.8 MB resolution. The camera lens mounted on the DSLR camera was a Tamron zoom lens with a focal length between 28 mm and 300 mm. We found through a preliminary experiment that the zoom lens had a depth of focus less than 10 cm and a distortion rate of less than 1%. Hence, we assumed that an image distortion occurring from the wave aberrations of the camera lens could be ignored.

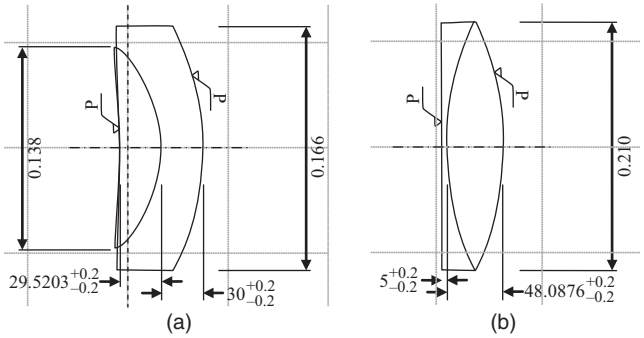

Fig. 5. Design specifications of converging optical system: (a) group 1 and (b) group 2.

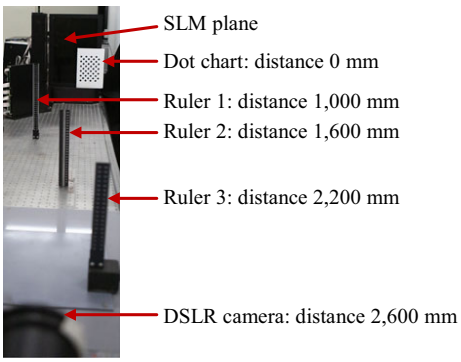

Fig. 6. Experimental configuration of viewing-window holographic display.

The 2D grid texture pattern in Fig. 7 was used for an object wave field $U(x_1, y_1)$ so that the distortion of the reconstructed image could be recognized.

We need to conduct an experiment on several viewing windows placed in different positions because wave aberrations are measured differently according to the position of the viewing window. We carried out an experiment on nine viewing windows, as shown in Fig. 8. The sampled locations are limited to ±100 mm in the x axis and ±100 mm in the y axis.

The Zernike coefficients on an exit pupil of a converging optical system are calculated according to (5) after obtaining a wave aberration function using the positions of the rays arriving on the viewing window. We can easily obtain the Zernike coefficients by using Zemax [28], a lens design tool. Tables 1 through 5 show the Zernike coefficients with regard to only five of nine positions. The Zernike coefficients in a viewing window with a position $(x_{vc}, y_{vc}) = (0, 0)$ in Table 1 indicate that only spherical aberrations exist in a converging optical system. The spherical aberration is the predominant one of the aberrations and mainly causes a barrel or a pincushion distortion in an image reconstructed from a hologram pattern in the position $(x_{vc}, y_{vc}) = (0, 0)$.

The converging optical system includes some tilts and an astigmatism in addition to spherical aberrations in terms of the viewing windows with off-axis positions, such as (−100, 100)(100, 100)(−100, −100), and (100, −100). The reconstructed hologram image appears somewhat oblique because both a tilt and astigmatism are dominant in the off-axis position. We can calculate a wave aberration field $P(x_s, y_s; x_{vc}, y_{vc})$ by using the Zernike coefficients according to (4) and (6).

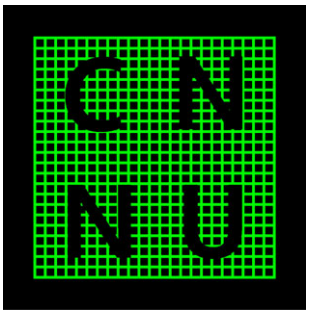

Fig. 7. 2D grid texture pattern $U(x_1, y_1)$ used for generating a hologram pattern.

https://doi.org/10.4218/etrij.17.0116.0049

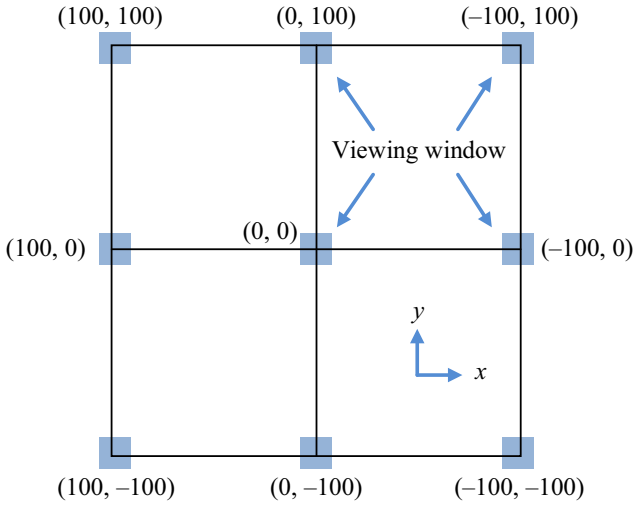

Fig. 8. Sampled locations of the viewing window.

We numerically generated a hologram pattern to be loaded on the SLM plane according to (12) in which $R_{vw}(x_2, y_2)$ on the retina plane is replaced with $U\left(-\frac{d_1}{d_2}x_2, -\frac{d_1}{d_2}y_2\right)$ on the object plane by (13). We obtained hologram patterns by specifically defining $U(x_1, y_1)$ as a 2D grid texture pattern, shown in Fig. 7, at a distance of 1,000 mm, 1,600 mm, or 2,200 mm from the SLM plane. We also set wavelength λ to 532 nm, d_s to 2,600 mm, d_1 to 1,600/1,000/400 mm, and d_2 to 25 mm in (12) for generating a hologram pattern. The radius r of the eye lens in the pupil aperture function $PL(x_{pc}, y_{pc}, r)$ of (9), (17) and 20 is set to 2 mm, and the pupil center (x_{pc}, y_{pc}) is assumed be located in a quarter position $(\lambda d_s/(4p_x), \lambda d_s/(4p_y))$ of the viewing window size $(\lambda d_s/(4p_x), \lambda d_s/(4p_y))$, where a pixel pitch (p_x, p_y) is (125 μm, 125 μm) in $SPF(x_s, y_s)$ of (15) and (18) to (21).

The optically reconstructed images from the hologram patterns in a viewing-window holographic display were captured by a DSLR camera placed at a position of the viewing window on the pupil plane. It was focused on the

Table 1. Zernike coefficients on a viewing window with center position $(x_{vc}, y_{vc}) = (0, 0)$.

Order	Frequency	Aberration	Zernike coefficient (@wavelength: 532 nm)	
			Wave number	μm
4	0	Spherical Aberration	1.97	1.05
6	0	Spherical Aberration	−2.46	−1.31

Table 2. Zernike coefficients on a viewing window with center position $(x_{vc}, y_{vc}) = (-100, 100)$.

Order	Frequency	Aberration	Zernike coefficient (@wavelength: 532 nm)	
			Wave number	μm
1	−1	Tilt in y axis direction	−1.16	−0.617
1	1	Tilt in x axis direction	1.16	0.617
2	−2	Astigmatism ±45°	−2.3	−1.22
4	0	Spherical Aberration	1.08	0.575
6	0	Spherical Aberration	−2.5	−1.33

Table 3. Zernike coefficients on a viewing window with center position $(x_{vc}, y_{vc}) = (100, 100)$.

Order	Frequency	Aberration	Zernike coefficient (@wavelength: 532 nm)	
			Wave number	μm
1	−1	Tilt in y axis direction	−1.16	−0.617
1	1	Tilt in x axis direction	−1.16	−0.617
2	−2	Astigmatism ±45°	2.3	1.22
4	0	Spherical Aberration	1.08	0.575
6	0	Spherical Aberration	−2.5	−1.33

Table 4. Zernike coefficients on a viewing window with center position $(x_{vc}, y_{vc}) = (-100, -100)$.

Order	Frequency	Aberration	Zernike coefficient (@wavelength: 532 nm)	
			Wave number	μm
1	−1	Tilt in y axis direction	1.16	0.617
1	1	Tilt in x axis direction	1.16	0.617
2	−2	Astigmatism ±45°	2.3	1.22
4	0	Spherical Aberration	1.08	0.575
6	0	Spherical Aberration	−2.5	−1.33

Table 5. Zernike coefficients on a viewing window with center position $(x_{vc}, y_{vc}) = (-100, -100)$.

Order	Frequency	Aberration	Zernike coefficient (@wavelength: 532 nm)	
			Wave number	μm
1	−1	Tilt in y axis direction	1.16	0.617
1	1	Tilt in x axis direction	−1.16	−0.617
2	−2	Astigmatism ±45°	−2.3	−1.22
4	0	Spherical Aberration	1.08	0.575
6	0	Spherical Aberration	−2.5	−1.33

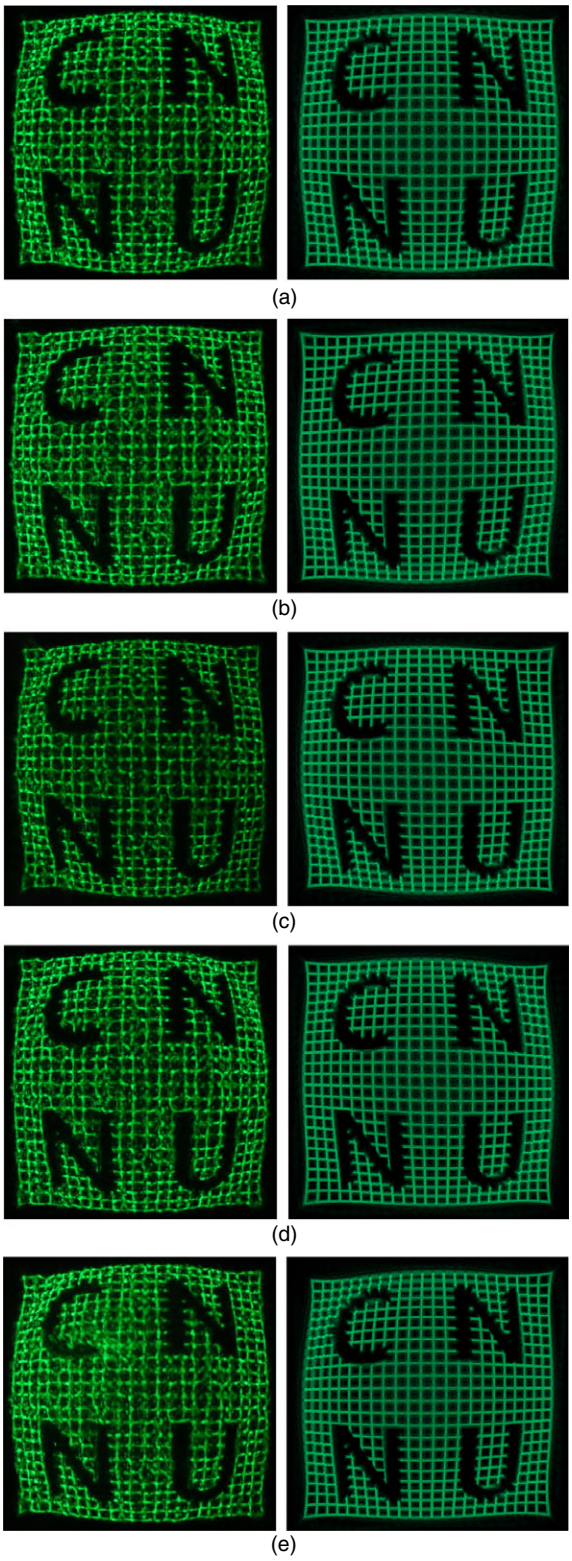

Fig. 9. Optical (left) and numerical (right) reconstructed images according to the viewing window position on the focus plane located at 2,200 mm from the SLM plane at center positions of (a) $(x_{vc}, y_{vc}) = (0, 0)$, (b) $(x_{vc}, y_{vc}) = (-100, 100)$, (c) $(x_{vc}, y_{vc}) = (100, 100)$, (d) $(x_{vc}, y_{vc}) = (-100, -100)$ and (e) $(x_{vc}, y_{vc}) = (100, -100)$.

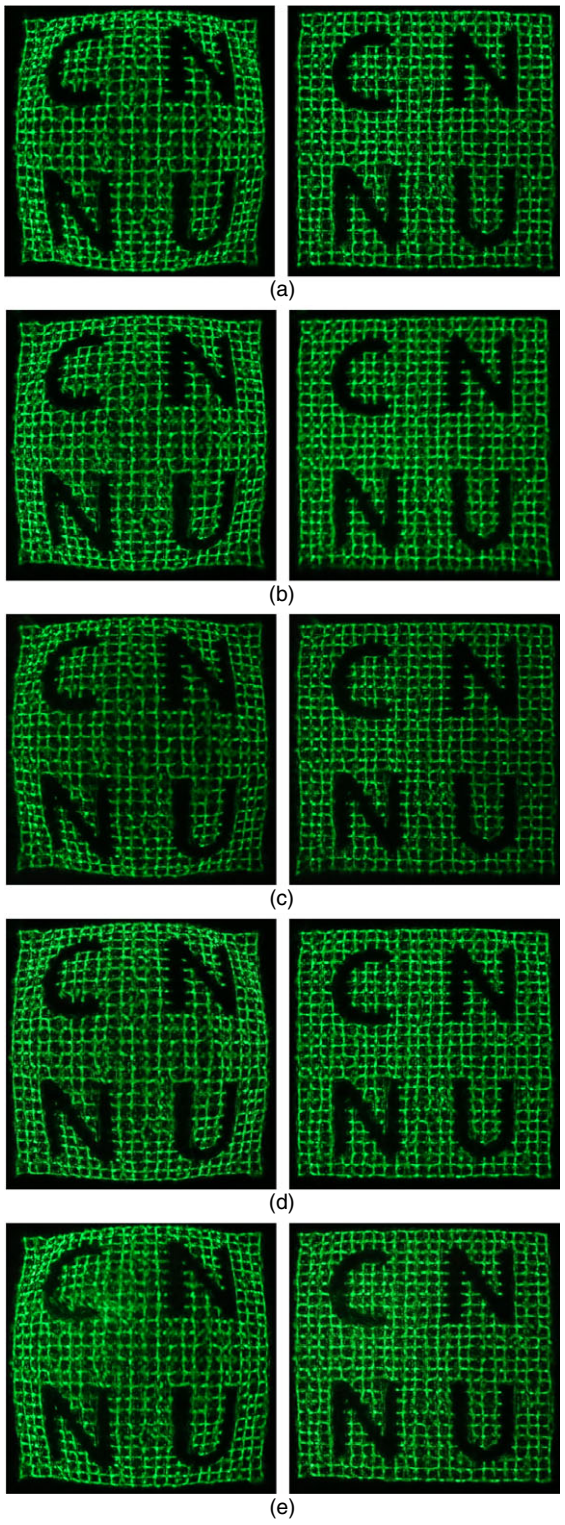

Fig. 10. Images reconstructed from a hologram without (left) and with (right) compensation on the focus plane located at 2,200 mm from the SLM plane at a center position of the viewing window of (a) $(x_{vc}, y_{vc}) = (0, 0)$, (b) $(x_{vc}, y_{vc}) = (-100, 100)$, (c) $(x_{vc}, y_{vc}) = (100, 100)$, (d) $(x_{vc}, y_{vc}) = (-100, -100)$ and (e) $(x_{vc}, y_{vc}) = (100, -100)$.

https://doi.org/10.4218/etrij.17.0116.0049

object plane located at a distance of 1,000 mm, 1,600 mm, or 2,200 mm from the SLM plane. The left-sided images in Fig. 9 show the reconstructed images at 2,200 mm from the SLM plane when the viewing window was placed at five positions: (0, 0)(−100, 100)(100, 100)(−100, −100) and (100, −100).

The images have a geometric distortion owing to wave aberrations caused by the converging optical system of a viewing-window holographic display. The distorted shape of each optically reconstructed image differs from the others because the kind of wave aberration occurs differently according to the position of the viewing window. We numerically simulate a reconstructed image with distortion by inputting a generated hologram pattern $D(x_s, y_s)$ and wave aberration field $P(x_s, y_s; x_{vc}, y_{vc})$ into (20), as shown in the right-side images of Fig. 9.

The distortion characteristics of the numerically calculated image are very close to those of the optically reconstructed image. Figure 9(a) shows the spherical aberration distortion when it is observed at the center position (0, 0) of a viewing window. Figures 9(b), (c), (d), and (e) illustrate the tilting distortion that the grid lines close to one corner are spread more flatly than those near to other corners. Figure 9 illustrates that the distortion patterns in the optical reconstruction images (left) and the numerical reconstruction images (right) are almost similar. This indicates that the wave aberrations calculated through ray-tracing are the approximately simulated real aberrations of the converging optical system in Fig. 6, which is the reason why we use the calculated wave aberration field $P(x_s, y_s; x_{vc}, y_{vc})$ for suppressing the distortion of a reconstructed image.

The right side of Fig. 10 shows the optically reconstructed images by using a hologram pattern $\bar{D}(x_s, y_s; x_{vc}, y_{vc})$, which was generated to compensate the distortion by assigning $P(x_s, y_s; x_{vc}, y_{vc})^{-1}$ into (21). In Fig. 10, the distorted grid lines of the left-side image are directly unfolded in the corresponding right-side image. It is additionally shown that the resolution of the reconstructed hologram images is improved because the aberration compensation for the phase error due to the optical system has the effect of deblurring the reconstructed hologram image through phase retrieval [30], [31].

Figure 11 shows the model used to calculate the distortion ratio for a numerical comparison between the

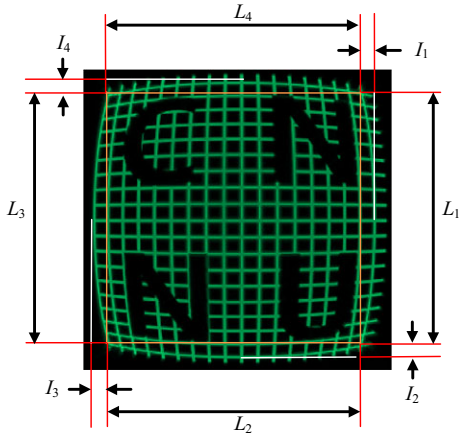

Fig. 11. Distortion ratio model.

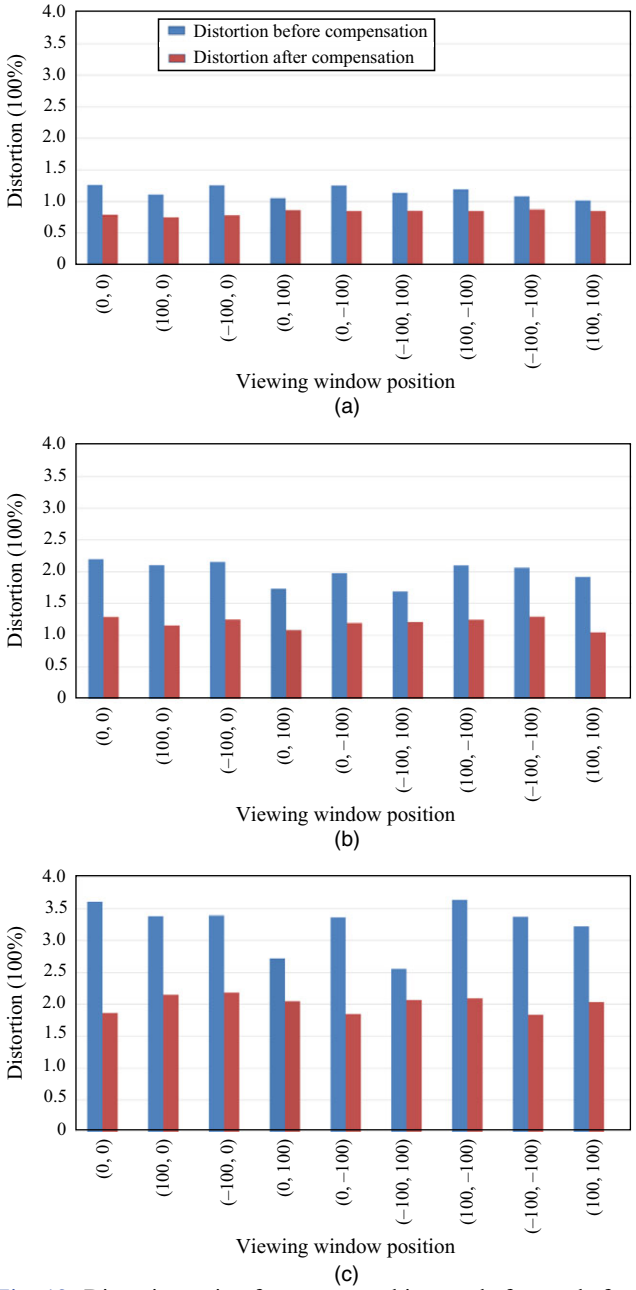

Fig. 12. Distortion ratio of reconstructed images before and after compensation with respect to the object plane placed at a distance of (a) 1,000 mm, (b) 1,600 mm, and (c) 2,200 mm from the SLM plane.

reconstructed images before and after compensation according to (23) [29].

We define a distortion ratio as an average of four ratios obtained by dividing the length of the maximum deviation between a straight line and a bending line by that of a straight line connecting both corner points in (23).

$$Distortion\ ratio = \left(\frac{I_1}{L_1} + \frac{I_2}{L_2} + \frac{I_3}{L_3} + \frac{I_4}{L_4}\right) \div 4 \times 100(\%). \quad (23)$$

Figure 12 illustrates the distortion ratio before and after compensation in the optically reconstructed images resulting from nine positions of the viewing window when the object plane is located at a distance of 1,000, 1,600, and 2,200 mm from the SLM plane according to (23). The average distortion ratio after compensation is decreased by 28%, 42%, and 38% compared with before the compensation on the object plane at a distance of 1,000, 1,600, and 2,200 mm, respectively.

V. Conclusion

In this paper, we proposed a numerical method to compensate the distortion of a reconstructed image from a hologram pattern displayed in a viewing-window holographic display. The method is implemented by deriving the diffraction model to numerically simulate wave aberrations of the converging optical system of a viewing-window holographic display. We demonstrated that, in our experimental configuration of a viewing-window holographic display, a numerical calculation independently decreases the distortion ratio of the reconstructed image by more than 28%.

The proposed approach enables effective suppression of the distortion with neither a change in the optical configuration nor the addition of an optical device in the viewing holographic display. This is because it enables a numeric compensation of the distortion with no additional effort when only the design specifications of the converging optical system are given.

Acknowledgement

This research was supported by GigaKOREA project grant (GK17D0100, Development of Telecommunications Terminal with Digital Holographic Table-top Display) and Institute for Information & communication Technology Promotion(IITP) grant funded by the Korea government (MSIT)(2017-0-00417, Openholo library technology development for digital holographic contents and simulation).

References

[1] M. Stanley et al., "100 Mega-Pixel Computer Generated Holographic Images from Active Tiling – a Dynamic and Scalable Electro-Optic Modulator System," *Proc. SPIE-IS&T*, vol. 5005, May 2003, pp. 247–258.

[2] Y. Takaki and N. Okada, "Hologram Generation by Horizontal Scanning of a High-Speed Spatial Light Modulator," *Appl. Opt.*, vol. 48, no. 17, 2009, pp. 3255–3260.

[3] J.K. Hahn et al., "Wide Viewing Angle Dynamic Holographic Stereogram with a Curved Array of Spatial Light Modulators," *Opt. Exp.*, vol. 16, no. 16, 2008, pp. 12372–12386.

[4] T. Kozacki et al., "Wide Angle Holographic Display System with Spatiotemporal Multiplexing," *Opt. Exp.*, vol. 20, no. 25, 2012, pp. 27473–27481.

[5] J.-Y. Son et al., "Holographic Display Based on a Spatial DMD Array," *Opt. Lett.*, vol. 38, 2013, pp. 3173–3176.

[6] S. Reichelt et al., "Holographic 3-D Displays- Elector-Holography within the Grasp of Commercialization," *Advances in Lasers and Electro Optics*, INTECH, 2010.

[7] M. Park et al., "Digital Holographic Display System with Large Screen Based on Viewing Window Movement for 3D Video Service," *ETRI J.l*, vol. 36, no. 2, 2014, pp. 232–241.

[8] E. Hecht, *Optics*, Addison-Wesley, 2002, pp. 253–266.

[9] J. Upatnieks, A. Vander Lugt, and E. Leith, "Correction of Lens Aberrations by Means of Holograms," *Appl. Opt.*, vol. 5, 1966, pp. 589–593.

[10] A. Stadelmaier and J.H. Massig, "Compensation of Lens Aberrations in Digital Holography," *Opt. Lett.*, vol. 25, 2000, pp. 1630–1632.

[11] P. Ferraro et al., "Compensation of the Inherent Wave Front Curvature in Digital Holographic Coherent Microscopy for Quantitative Phase-Contrast Imaging," *Appl. Opt.*, vol. 42, 2003, pp. 1938–1946.

[12] T. Colomb et al., "A Numerical Parametric lEns for Shifting, Magnification and Complete Aberration Compensation in Digital Holographic Microscopy," *J. Opt. Soc. Am. A*, vol. 23, 2006, pp. 3177–3190.

[13] M. Paturzo and P. Ferraro, "Creating an Extended Focus Image of a Tilted Object in Fourier Digital Holography," *Opt. Exp.*, vol. 17, no. 22, 2009, pp. 20546–20552.

[14] P. Ferraro et al., "Controlling Depth of Focus in 3D Image Reconstructions by Flexible and Adaptive Deformation of Digital Holograms," *Opt. Lett.*, vol. 34, 2009, pp. 2787–2789.

[15] M. Paturzo et al., "Synthesis and Display of Dynamic Holographic 3D Scenes with Real-World Objects," *Opt. Exp.*, vol. 18, no. 9, 2010, pp. 8806–8815.
[16] P. Memmolo et al., "Automatic Focusing in Digital Holography and its Application to Stretched Holograms," *Opt. Lett.*, vol. 36, 2011, pp. 1945–1947.
[17] T. Shimobaba et al., "Lensless Zoomable Holographic Projection Using Scaled FRESNEL Diffraction," *Opt. Exp.*, vol. 21, no. 21, 2013, pp. 25285–25290.
[18] T.K. Uhm et al., "A Study on the Actuator Arrays of a Deformable Mirror for Adaptive Optics," *Opt. Soc. Korea*, vol. 13, no. 5, 2002, pp. 442–448.
[19] M.J. Booth, "Adaptive Optics in Microscopy," *Philosophical Trans. Royal Soc.*, vol. 365, 2007, pp. 2829–2843.
[20] H. Gross, *Handbook of Optical systems*, vol. 2, Wiley-VCH, 2007, pp. 212–216.
[21] R. Navarro, R. Rivera, and J. Aportab, "Representation of Wavefronts in Free-form Transmission Pupils with Complex Zernike Polynomials," *J. Opt.*, vol. 4, no. 2, 2011, pp. 41–48.
[22] B.C. Platt and R. Shack, "History and Principles of Shack-Hartmann Wavefront Sensing," *J. Refract. Surg.*, vol. 17, no. 5, 2001, pp. S573–S577.
[23] H. Gross, *Handbook of Optical Systems*, vol. 1, Wiley-VCH, 2007, pp. 782–786.
[24] O. Cugat et al., "Deformable Magnetic Mirror for Adaptive Optics: Technological Aspects," *Sensors Actuators A*, vol. 89, no. 1–2, 2001, pp. 1–9.
[25] T.K. Uhm et al., "A Study on the Actuator Arrays of a Deformable Mirror for Adaptive optiCs," *Opt. Soc. Korea*, vol. 13, no. 5, 2002, pp. 442–448.
[26] J. W. Goodman, *Introduction to Fourier Optics – 3rd edition*, Roberts & Company, 2005, pp. 109–115.
[27] E. Cuche, P. Marquet, and C. Depeursinge, "Spatial Filtering for Zero-Order and Twin-Image Elimination in Digital Off-axis Holography," *Appl. Opt.*, vol. 39, no. 23, 2000, pp. 4070–4075.
[28] Zemax, Accessed 2016, http://www.zemax.com/
[29] Michel. Thoby, "How is Lens Distortion Value Being Defined by the Industry and by Some International Standardization Groups?" Accessed 2016. http://michel.thoby.free.fr/Fisheye_history_short/International_Standards_about_Distortion.html
[30] Y. Hao and A. Asundi, "Resolution Analysis of a Digital Holography System," *Appl. Opt.*, vol. 50, no. 2, 2011, pp.183–193.
[31] P. Ferraro et al., "Phase Map Retrieval in Digital Holography: Avoiding the Under Sampling Effect by a Lateral Shear Approach," *Proc. SPIE*, vol. 6995, 2008, pp. 6995061–6995066.

Minsik Park received his BS degree in electrical engineering from Kwangwoon University, Seoul, Rep. of Korea, in 1997, his MS degree in mechatronics engineering from Gwangju Institute of Science and Technology, Gwangju, Rep. of Korea, in 1999, and his PhD degree in computer science and engineering from Chungnam National University, Daejeon, Rep. of Korea, in 2016. Since 1999, he is currently working as a Principal Researcher in ETRI, Daejeon, Rep. of Korea. His research interests include signal and image processing, machine learning, and holography.

Hyun-Eui Kim received his BS and MS degrees in information and communication engineering from Chungbuk National University, Cheongju, Rep. of Korea, in 2010 and 2012, respectively. Since 2012, he has been working at ETRI, Daejeon, Rep. of Korea. His research interests include digital holography and light field 3D display system.

Hyon-Gon Choo received his B.S. and M.S. degree in electronic engineering in 1998 and 2000, respectively, and his Ph.D degree in electronic communication engineering in 2005 from Hanyang University, Seoul, Rep. of Korea. He is currently working as a Principal Researcher in ETRI, Daejeon, Rep. of Korea. His research interests include holography, multimedia protection, and 3D broadcasting technologies.

Jinwoong Kim received his BS and MS degrees in electronics engineering from Seoul National University, Seoul, Rep. of Korea, in 1981 and 1983, respectively. He received his PhD degree in electrical engineering from Texas A&M University, College Station, TX, USA, in 1993. He has been working in ETRI, Daejeon, Rep. of Korea since 1983, leading many projects in the telecommunications and digital broadcasting areas.

Cheong Hee Park received her Ph.D. in Mathematics from Yonsei University, Seoul, Rep. of Korea in 1998. She received the M.S. and Ph.D. degrees in Computer Science at the Department of Computer Science and Engineering, University of Minnesota, USA in 2002 and 2004 respectively. She is currently in the dept. of Computer Science and Engineering, Chungnam National University, Daejoen, Rep. of Korea as a professor. Her research interests include data mining, machine learning, and pattern recognition.

https://doi.org/10.4218/etrij.17.0116.0049